Aerospace Science and Technology 58 (2016) 71–81

Contents lists available at ScienceDirect

Aerospace Science and Technology

www.elsevier.com/locate/aescte

The effect of sweep on flowfields of a highly loaded transonic rotor

Weiwei Cui [a], Xiaorong Xiang [a], Qingjun Zhao [a,b,*], Jianzhong Xu [a]

[a] Institute of Engineering Thermophysics, Chinese Academy of Sciences, China
[b] Key Laboratory of Light-Duty Gas-Turbine, Chinese Academy of Sciences, No. 11 Beisihuan West Road, Beijing, 100190, China

ARTICLE INFO

Article history:
Received 26 October 2014
Received in revised form 19 May 2016
Accepted 1 August 2016
Available online 8 August 2016

Keywords:
Aerodynamic sweep
Internal blade loading match
Radial equilibrium
Stall margin

ABSTRACT

A new view of internal blade loading match is employed in this paper to reveal the essential relationship between sweep and complicated flow phenomenon in compressors. A forward swept rotor named as SF and an aft swept rotor named as SA, are designed originating from NASA Rotor 37. The numerical results indicate the isentropic efficiency and total pressure ratio of the new rotor with forward sweep are a little larger than rotor Baseline at peak efficiency point, and its stall margin has an over 10% increase as well. By contrast, the opposite change appears in the aft swept rotor SA. In addition, the choking massflow of swept rotors changes clearly as a result of the spatial change of aerodynamic throat and the forward sweep produces a larger throat area and choking massflow. A noted phenomenon is shown that both forward and aft sweep benefit a certain range of blade span for flow characteristic improvement, and the sweep also affects the inflow condition, 3-D shock structure and internal loading distributions of swept rotors. Both the new radial equilibrium in flowfield and transportation of low-energy fluids in boundary layer induced by sweep appear conductive to reduce shock wave and flow blockage in tip region of forward swept rotor SF. Meanwhile, the strength of leakage flow is also suppressed in the forward swept rotor SF because of the decreased blade loading near leading edge in tip region. In fact, all the change in swept rotors tends to be a new characteristic match of blade airfoil at different span, and the re-matching of flow characteristic for blade airfoil determines the stable operation range and the overall performance of swept rotors at design point directly.

1. Introduction

Increasing stage pressure ratio of compressor is one of the key methods to improve thrust-weight ratio of advanced aero-engine. Nevertheless, the overall performances of highly loaded compressors seem to be constrained by deteriorated stall margin and off-design characteristics when stage loading increases [1]. As is known, complicated flow phenomenon exists in high loading transonic compressor, and has much closer relationship with flow unsteadiness, such as the interactions among leakage vortex, passage shock and boundary layer [2–4]. As a result, the flow in high loading compressors is sensitive to geometry of blade airfoil at different span, and larger challenges have emerged inevitably for blade optimal design [5]. In light of successful application of back-swept aircraft wing technique, researchers found that it's wise to introduce lean\sweep into design to control endwall separation, reduce losses of shock and secondary flow, and improve the operation range of compressors [6,7]. The studies on lean/sweep were carried out in subsonic compressor originally, and then extended to transonic and supersonic compressors [8,9]. Fortunately, it has been proven to be an effective method to improve the overall performance of highly loaded compressors [10]. Beatty [11] and Goldwin [12] first began to analyze the effect of aft sweep on the characteristics of compressor rotors and cascades. During the same period, Smith and Yeh [13] provided intuitive and systematical definition of leaned and swept blade, which is beneficial to use lean/sweep into optimal design of compressor. The aft sweep was preferred to reduce strong shock wave and noise in earlier study of compressors. In the mid of 1970s, researchers in NASA designed and tested a fan with highly aft swept leading edge, which is named as QF-12 [14]. Although the overall performance of aft swept fan was lower than the design goal, the operation noise of blade reduced obviously. During the period of 1966 to 1968, engineers in GE Company [15] tried to design swept rotors for the fan stages of engine TF39, and simple linear sweep was applied into optimal design.

In order to make use of the merit of sweep in shock control for compressors, a new program was carried out in Wright laboratory of US during 1980s, and an aft swept transonic rotor was designed to test and analyze the effect of sweep on efficiency of

* Corresponding author at: Key Laboratory of Light-Duty Gas-Turbine, Chinese Academy of Sciences, No. 11 Beisihuan West Road, Beijing, 100190, China.
E-mail addresses: cuiweiwei@iet.cn (W. Cui), zhaoqingjun@iet.cn, qingjunzhao@163.com (Q. Zhao).

http://dx.doi.org/10.1016/j.ast.2016.08.002
1270-9638/

Nomenclature

Abbreviation

PS	Pressure surface
SS	Suction surface
LE	Leading edge
TE	Trailing edge

Symbols

G	Massflow	kg/s
ρ	Density	
σ	Solidity	
r	radius	m
$W1$	Inlet flow velocity in rotating frame of reference	
$W2$	Outlet flow velocity in rotating frame of reference	
C_θ	Tangential component of velocity into blade row	
Ca	Axial component of absolute velocity	m/s
A	Cross-sectional area	m^2
A_{th}	Throat area	m^2
C	Absolute velocity	m/s
Ma_{re}	Relative Mach number	
Ma_{th}	Relative Mach number at throat	
P^*_{th}	Relative total pressure at throat	
T^*_{th}	Relative total temperature at throat	
$q(Ma)$	Flux function	
P	Static pressure	Pa
T	Static temperature	K
$P_{0,in}$	Inlet absolute total pressure	Pa
$T_{0,in}$	Inlet absolute total temperature	K
K	Constant, $\sqrt{\frac{k}{R}(\frac{2}{k+1})^{\frac{k+1}{k-1}}}$	
$\overline{G}$	Corrected massflow, $\frac{G\cdot\sqrt{T_{0,in}}}{P_{0,in}}$	

rotor. Hah and Wennerstrom [6] analyzed the internal flow of aft swept rotor in detail, and found that the shape of shock front near suction surface of swept rotor tends to be aft sweep as well. Besides that, a strong radial transport of low-energy fluids exists in boundary layer near suction side of aft swept rotor. Hah and Puterbaugh [16] found the overall performance of transonic rotor can be affected by aerodynamic sweep via two ways. The first is the change of distance between leading edge and passage shock in tip region of swept rotor, and the second is the radial transportation and accumulation of low-energy fluids in boundary layer near suction side, which is closely related to the flow blockage in tip region of rotor. Bergner and Kablitz [17] compared the shock structure in swept rotors, and found that the shock front over mid-span of the forward swept rotor goes much more downstream in passage, but the aft tendency of shock front disappears near casing. Shan [18] revealed the relationship between leading edge curve and shock front in blade passage, and found that sweep structure of leading edge affects the shock wave and the aerodynamic parameters behind shock front.

The most impressive merit of aerodynamic sweep is that it benefits the stall margin in high loading compressors. Wadia and Szucs [19] found that the peak efficiency and stall margin of forward swept rotor are much better than original unswept rotor, while the stall margin of aft swept rotor gets worse significantly. Denton and Xu [20] found that the effects of lean and sweep on pressure ratio and isentropic of rotors are not obvious, but it does have a significant influence on the characteristic of near stall condition. They also revealed the shock front always tends to be perpendicular to the casing, so the forward swept rotor produces a good stall margin with the passage shock downstream away from the leading edge. Yamaguchi and Tominaga [21] illustrated that the low-energy fluids in boundary layer transport from hub to tip in radial direction driven by both centrifugal stress and radial pressure gradient in blade, and the losses and stall margin of compressor are determined by the accumulation of low-energy fluids near suction side. Ramakrishna and Govardhan [22] showed that the forward sweep produces large operation range because that it attenuates the accumulation of low-energy fluids in boundary layer significantly and further reduces flow separation and the number of stall cells in tip region of blad. Sasaki and Breugelmans [23] revealed as well that aerodynamic sweep has been conductive to attenuate secondary flow, reduce the corner separation, and improve the stall margin of compressors. In addition, many benefits have been present due to the application of aerodynamic sweep into blade design. Watanabe and Zangeneh [24] introduced sweep into inverse design of compressor blade, and adjusted the span loading distribution simultaneously to complement the loading deficiency. Hidetaka [25] considered the sweep as a key control parameter in multi-objective optimization for compressor blade, and the results showed the efficiency and stall margin of new rotor have been improved obviously with no change in blade geometry. Aziz and Owis [26] optimized a transonic-fan rotor through lean and sweep, together with adjustment of thickness and camber distribution for blade airfoil. The results indicated the pressure ratio of new blade increases from 1.427 to 1.627 at the design point. Ayhan and Erkan [27] found that the forward and backward sweep do not significantly affect the overall performance of the fan at the design flow rate. However, at low flow rates, the sweep has double influences on the fan performance respectively. Janos [28] combined the controlled vortex method and forward sweep into optimal design, and found that both the losses away from the endwalls and effects of wall skin friction in fan blade have been reduced obviously. The study by Seyed and Masoud [29] showed as well both the sweep and lean angle benefit efficiency and sound pressure in an Axial-Flow Fan. Hah and Shin [30] found the flow in transonic rotor is much more stable because of composite sweep. Ji and Chen [10] viewed the sweep as a degree of freedom in design of compressors to reveal the advantages of sweep. However, Benini and Biollo [31] designed 26 rotors with sweep and lean through and illustrated the characteristics of aft swept rotors seem to be much better than forward swept rotors, and the finding is reversed to traditional knowledge of aerodynamic sweep.

In conclusion, the flow phenomenon produced by sweep has been illustrated in many literatures, and the advantages of aerodynamic sweep have been widely explored in blade design. However, as the blade loading increases, the essential relationships between aerodynamic sweep and complicated flow phenomenon require thorough understanding to clarify the negative effects and confusion for the use of sweep in turbomachinery. Therefore, the physics of aerodynamic sweep effects on high loading transonic rotors are illustrated from a new view of blade loading match in this paper, and some interesting findings are also present.

2. Design method

2.1. Investigated transonic rotor

The swept rotors studied in this paper are designed originating from an axial compressor rotor, NASA Rotor 37. Both the geometry data and experimental data of Rotor 37 were described in NASA report and AGARD report, and they have been open in public for

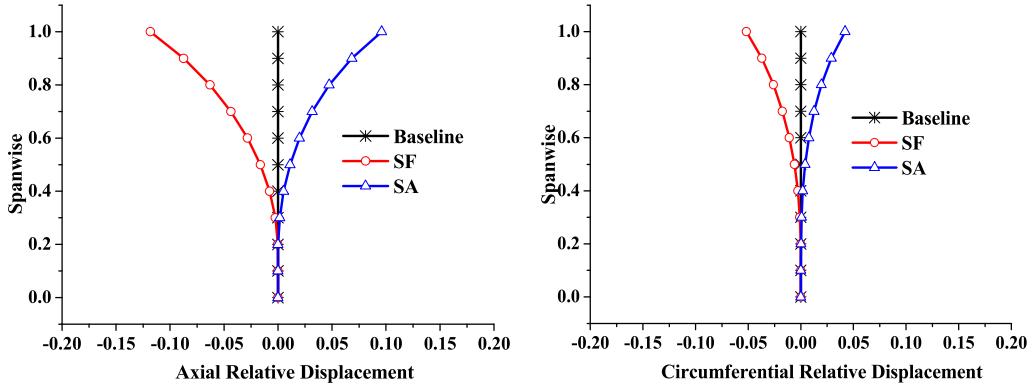

Fig. 1. The relative displacements of the controlled points.

Table 1
Key design parameters of tested Rotor 37.

Massflow at design point (kg/s)	20.19
Total pressure ratio at design point	2.106
Rotational speed (Rpm)	17188.7
Inlet relative Mach number	1.13 ~ 1.48
Blade number	36
Radius of blade tip (mm)	252
Aspect ratio	1.19
Solidity at blade tip	1.29
Tip clearance (mm)	0.356
Hub-tip ratio	0.7

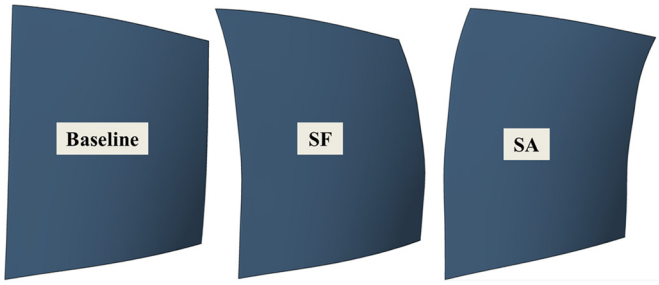

Fig. 2. Blade geometries.

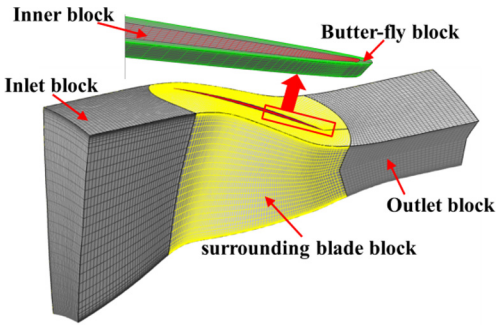

Fig. 3. Topological structures of grids.

decades [33,34]. The detailed design parameters of Rotor 37 are summarized in Table 1.

2.2. Design method of swept rotors

The forward swept rotor SF and aft swept rotor SA are designed by translating the centroids of Rotor 37 forward and backward respectively along local chordwise direction, with the geometry of blade airfoil unchanged. In order to determine the shape of stacking axis, ten controlled points, which correspond to the centroid of each blade airfoil, are set in radial direction from 10% to 100% span of Rotor 37. The new stacking axis generates by adjusting the displacement of controlled points along each chordwise direction. In consideration of larger losses and complicated flow phenomenon existing in tip region of rotor, the sweep mainly concentrated on elements above the 40% span of rotor, with the largest displacement in tip region. Specifically to the forward swept rotor SF, the 60% span section is moved forwards by 3% of its chord, the 80% section forwards by 7% its chord, and the 100% section forwards by 16% its chord. The stacking axis of aft swept rotor SA generates in the same way but has opposite translating direction and different displacement to the rotor SF (2%, 5% and 13% of chord at corresponding span of rotor). After several adjustments of the controlled points, the optimized stacking lines of swept rotors are established by jointing together all the controlled points smoothly with B-spline curves. In fact, the chordwise displacement of each blade section is obtained by decomposing it into axial and circumferential components respectively. Fig. 1 shows the two components of relative displacement at different span of blade, and the geometries of three rotors are illustrated in Fig. 2.

3. Numerical analysis method

3-D steady numerical calculations are performed on rotors employing the commercial CFD software FINE Turbo by NUMECA International. The RANS equations are discretized in space using cell centered control volume approach and in time using explicit multi-stage Runge–Kutta scheme. The typical two-equation SST turbulent model is employed in numerical solver and the multi-grid technique is used to accelerate the convergence of the flow solver to steady state [32]. The 3-D meshes of rotors are generated using the AutoGrid5 developed by NUMECA International as well. The calculation domain is divided into five different blocks with HOH topological structures to ensure higher gird quality. Three blocks located in main flow domain are named as inlet block, outlet block and surrounding blade block respectively. Similarly, the other two blocks located in clearance domain are named as inner block and butter-fly block, which is shown in Fig. 3. In order to improve the reliability of numerical analysis, the gird number of 1,600,000 and 1×10^{-6} m of first cell width near solid wall are chosen in mesh generation to ensure the $y^+ < 1$. Total pressure, total temperature and absolute flow angle are given on the inlet condition. Non-slip, non-penetration and adiabatic wall boundary condition are given on blade surface, hub, shroud and other solid wall. Besides that, the rotational speed of hub wall can be set as the same to rotating frame, and the shroud wall can be set to be stationary conveniently for numerical calculation in the solver of FINE Turbo.

In addition, the operation range of rotor in calculation is obtained through adjusting the back pressure of exit. The stalling point of rotor is taken to be the point at which the calculation diverges with a certain high back pressure (this is one of the most

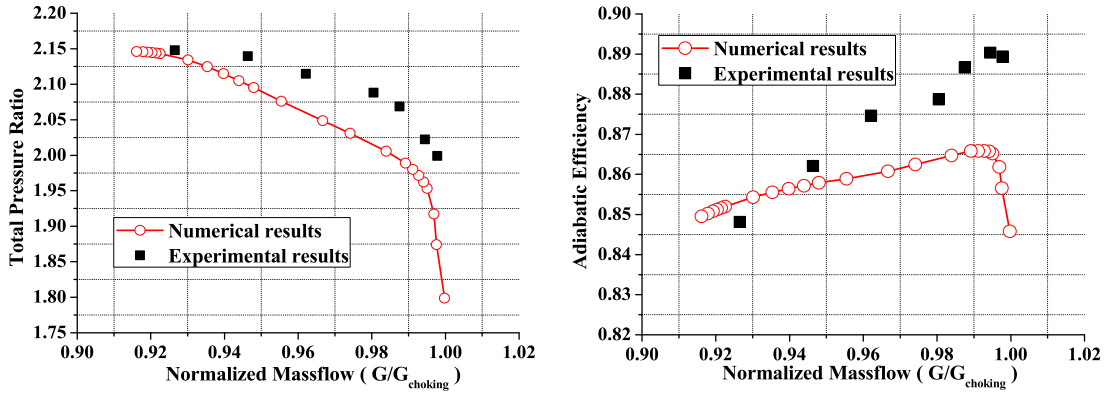

Fig. 4. Overall performance of Rotor 37 at design condition (rotational speed 17188 rpm, Tip gap 0.356 mm).

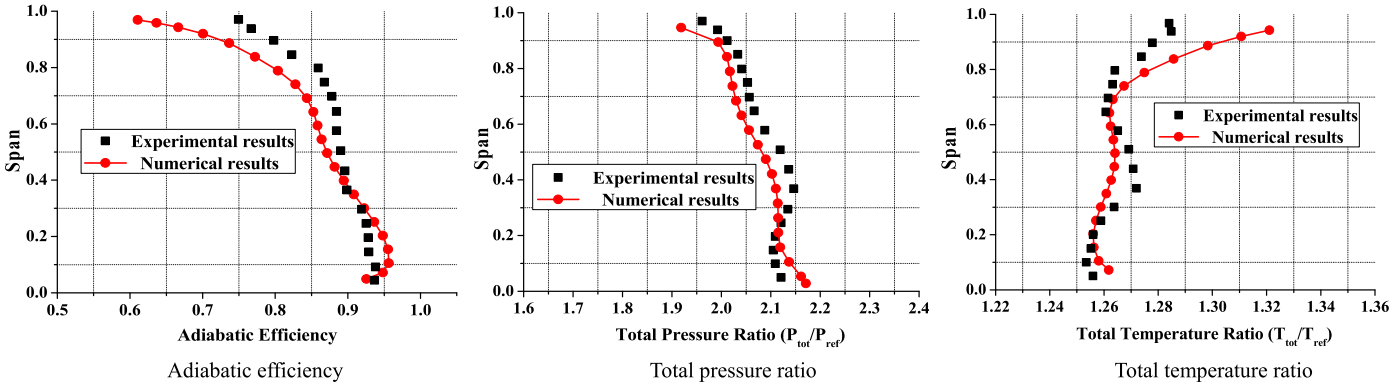

Fig. 5. Spanwise distributions of key parameters at 98% choke flow in Rotor 37.

common ways to predict the stall boundary of compressor in numerical calculation). As the mass flow decreases with increment of static pressure at exit, the convergence of calculation becomes difficult which may go through thousands of time steps. The stalling point obtained in this way is a best guess of when calculation failure occurs and it's feasible to view it as an indication of stall inception.

The comparisons between numerical results and detailed experimental data of Rotor 37 are shown in Fig. 4 and Fig. 5. Both the total pressure ratio and adiabatic efficiency in numerical method seem a little lower than the experimental results, but the maximum deviation of two methods are no more than 4%, and the same tendency of characteristic lines is present in Fig. 4. The spanwise distributions of adiabatic efficiency, total pressure ratio and total temperature ratio seem to be similar in two methods with a little larger difference near endwall of blade (viscous effects near solid wall), which is shown in Fig. 5.

The contours of relative Mach number shown in Fig. 6 indicate that the detailed flowfields of Rotor 37 has been described in numerical calculation compared with experimental results (including the shock structure and tip clearance effects). In conclusion, all the analyses above have well proved that the numerical method used in this paper has enough accuracy and satisfies the acquirement of calculation absolutely.

4. Results analysis

4.1. Effects of sweep on overall performance

The predicted overall performances of rotor Baseline, SF and SA are plotted against normalized massflow in Fig. 7. It shows that both the total pressure ratio and isentropic efficiency of rotor SF are larger than rotor Baseline at peak efficiency point, while it presents an opposite change in rotor SA. More important is that the stall margin of rotor SF has increased over 10%, while rotor SA reduces almost 15%, compared with the unswept rotor Baseline. It indicates the forward sweep behaves better to improve the stable operation range and overall performance of high loading compressor, and the aft sweep has much negative effects for rotor. In fact, the stall margin of compressor rotor is determined by the characteristics of design point and near stall point, so the better characteristics of the two points attribute to reasonable match of each elemental airfoil in blade span necessarily.

In addition, the choking mass flow of rotor SF has increased over 0.75% than rotor Baseline, but rotor SA reduces over 0.95% at the same condition. It means the maximum flux capacity of transonic rotor has changed due to aerodynamic sweep. As known in equation (1) that the massflow has direct relation to axial velocity–density when the inlet flow area of rotor is fixed (the same axial location is chosen as a reference position), so the spanwise distributions of axial velocity–density at the same axial position near entrance may well reflect the massflow change of three rotors at choking condition. It can be seen from Fig. 8 the change of axial velocity–density mainly concentrates on the outer half part of blade, and the rotor SF has the largest values in that range among three rotors. On the other hand, the choking massflow of rotor is determined by the maximum flux capacity of aerodynamic throat, and the location of throat can be described by the cross-section with Mach number equals to 1.0. The equation (2) indicates that the flux capacity of aerodynamic throat is related to the relative total temperature, relative total pressure and throat area in rotors. The distribution of relative total temperature is almost the same for three rotors in Fig. 9, so the relative total pressure and the area of aerodynamic throat play an important role in the choking massflow of rotors. As shown in Fig. 9, the relative total pressure of rotor SF is a little larger than rotor Baseline in outer 10% and in-

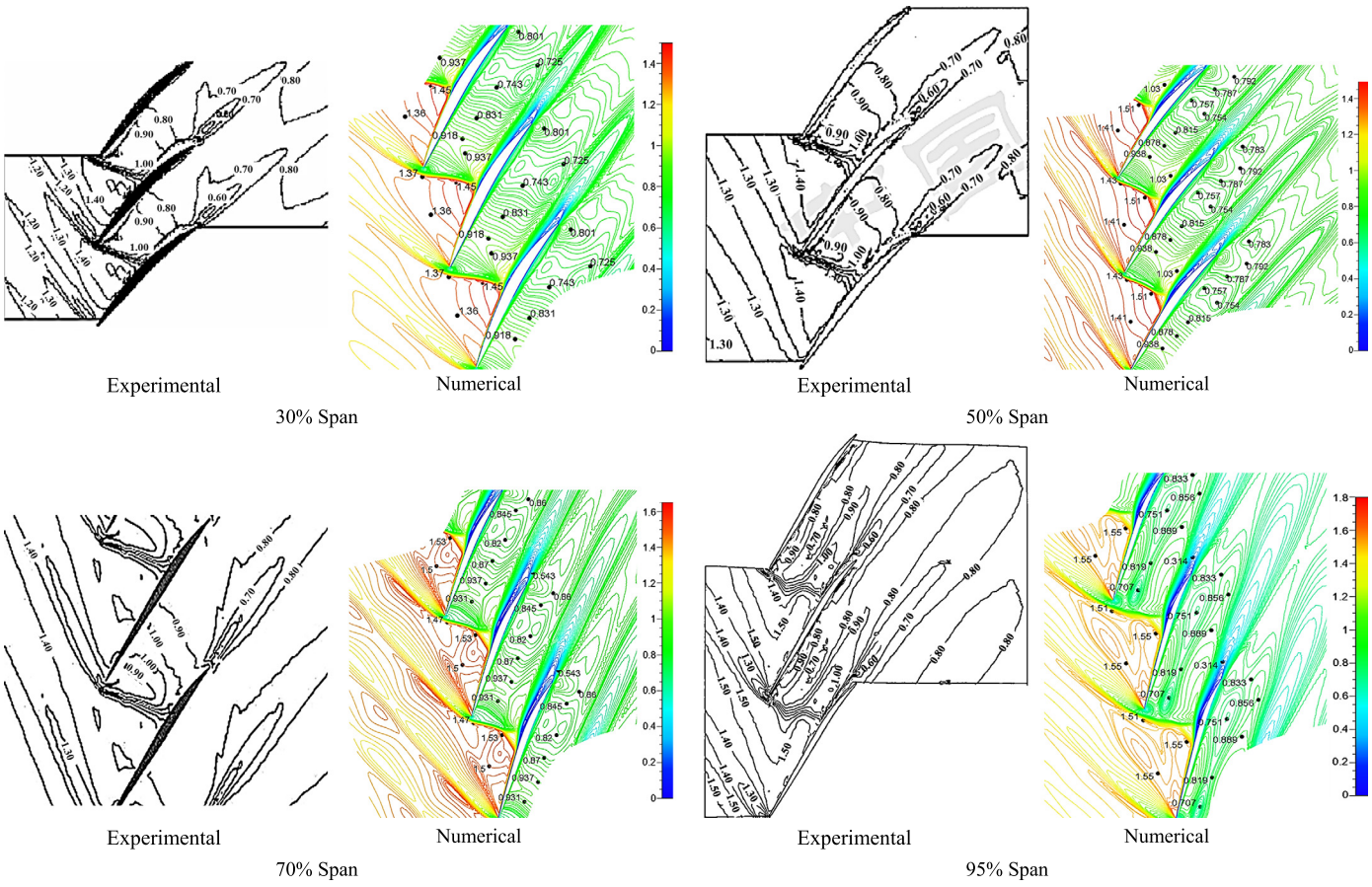

Fig. 6. Relative Mach number contours at 98% choke flow in Rotor 37. (For interpretation of the colors in this figure, the reader is referred to the web version of this article.)

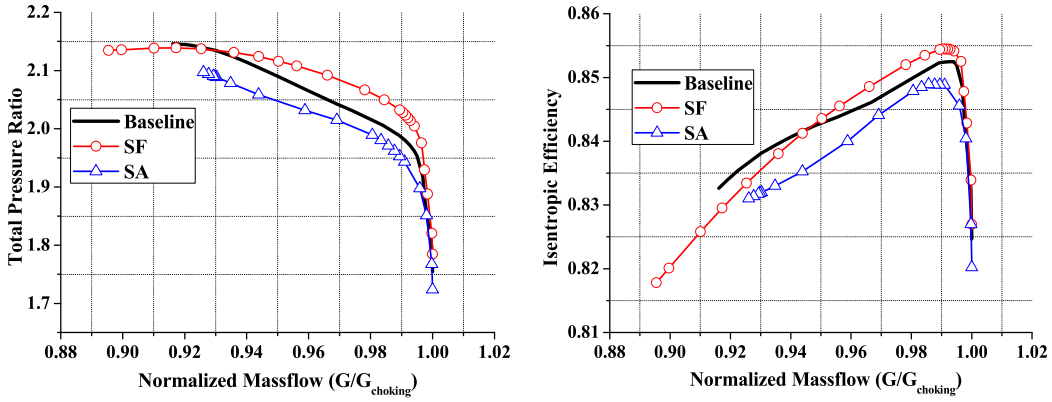

Fig. 7. Characteristics of rotor Baseline, SF and SA.

ner 20% blade span, but is smaller in the range of 20%∼40% span at choking condition. In comparison, the opposite change appears near the aerodynamic throat of rotor SA. Nevertheless, the differences of average relative total pressure at aerodynamic throat tend to be much less in three rotors.

$$G = \rho \cdot C_a \cdot A \quad \text{(axial intake at entrance)} \tag{1}$$

$$G = K \cdot \frac{P^*_{th}}{\sqrt{T^*_{th}}} \cdot A_{th} \cdot q(Ma_{th}) \quad \text{(at throat section)} \tag{2}$$

The black lines in Fig. 10 represent the distributions of relative Mach number with the value of 1.0 at different span of blades, which indicate the spatial distribution of aerodynamic throat in three rotors. As known the blade passage tends to be divergent from the largest thickness point to trailing edge in streamwise direction, so the more downstream away from leading edge the aerodynamic throat moves the larger throat area of rotor it means. The sonic lines in Fig. 10 obviously indicate the largest throat area exists in blade passage of rotor SF, while the area of aerodynamic throat is the smallest in rotor SA. Therefore, it's concluded the change of choking massflow in swept rotors is mainly related to the area change of aerodynamic throat produced by sweep, and the forward sweep may increase the throat area obviously, which is the main reason for the largest choking mass flow of rotor SF.

Fig. 11 shows the spanwise distributions of isentropic efficiency at peak efficiency point of three rotors. The total to total efficien-

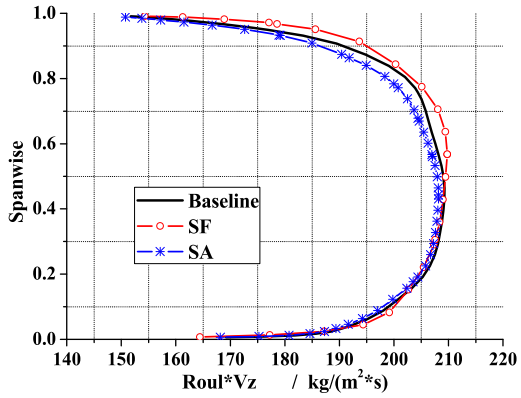

Fig. 8. Distributions of axial velocity–density on inlet of rotors at choking condition (with the same axial location).

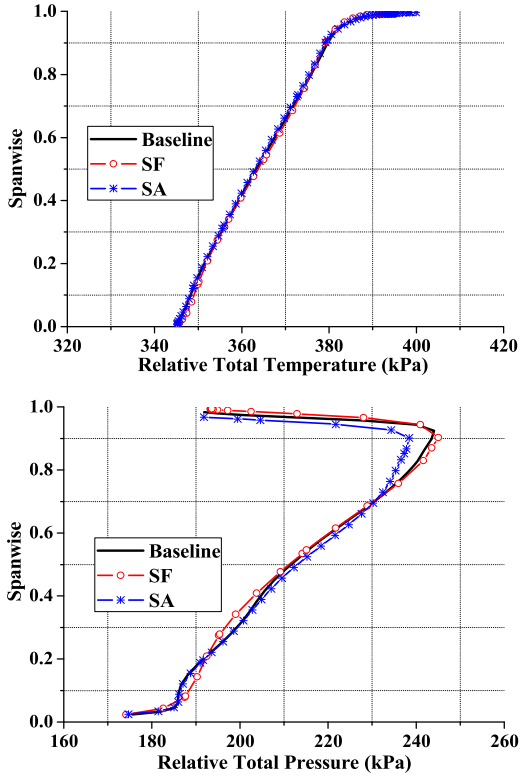

Fig. 9. Distributions of relative total temperature and relative total pressure near aerodynamic throat of rotors at choking condition.

cies are almost the same below 40% span of three rotors, but large change appears in outer 50% span. The efficiency of rotor SF is smaller than rotor Baseline in the region of 10%∼40% spans of blade, but improves obviously over 50% blade span. On the contrary, the efficiency of rotor SA near mid-span region is better than Baseline, but deteriorates in tip region. So it's noted that the sweep has different influence on blade airfoil at different span and it benefits a certain span range of rotors, so the overall efficiency of the swept rotor has not much larger improvement in comparison with unswept rotor.

4.2. Effects of sweep on flowfields

Fig. 12 shows the contours of relative Mach number at different span of blades at peak efficiency point. The stacking lines have little change below 30% blade span, so the flowfields are nearly the same in that region of three rotors. However, the intensity and

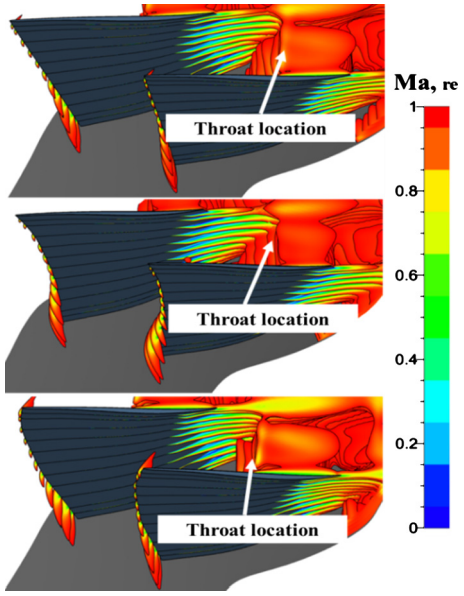

Fig. 10. The location of aerodynamic throat in three rotors at choking condition. (For interpretation of the colors in this figure, the reader is referred to the web version of this article.)

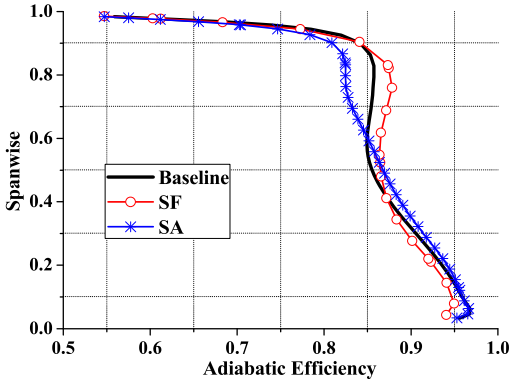

Fig. 11. Spanwise distributions of isentropic efficiency at peak efficiency point.

location of shock in passage are significantly influenced by sweep effects over 40% span of rotor. A bow shock near leading edge can be seen at 50% span of three rotors shown in Fig. 12. The passage shock is much farther away from leading edge in rotor SA, and its strength is much weaker as well. Therefore, the efficiency of rotor SA near mid-span is a littler larger than the other two rotors shown in Fig. 11. As the inlet relative Mach number increases, the strength of passage shock tends to be much larger in tip region of rotor. At 90% blade span, a much stronger shock forms near the leading edge of three rotors. More specifically, the passage shock in tip region of rotor SF weakens obviously due to forward sweep, and the location of shock is much more downstream than rotor Baseline. On the contrary, the shock near the leading edge of rotor SA is much stronger than rotor Baseline at 90% blade span. As a result, the isentropic efficiency of rotor SF is much higher in tip region due to its weaker shock. As the shock wave is the main way to increase static pressure in tip region of rotors, so the change of shock characteristic may inevitably affect the blade loading distribution. In this way, the loading of rotor SF increases at mid-span but decreases in tip region, which is opposite to the loading change in rotor SA. So it's evident from the change of passage shock at different blade span that aerodynamic sweep induces a new spanwise distribution of blade loading, and affects the shock losses and flow separation as well. In addition, a larger low-velocity region gener-

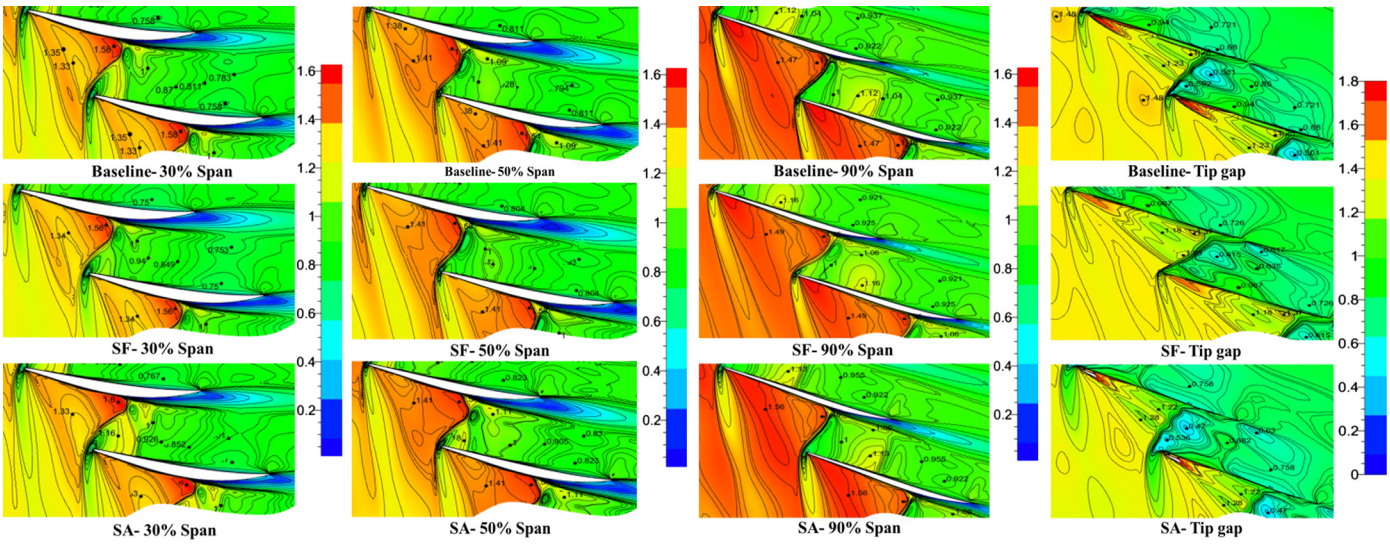

Fig. 12. Contours of relative Mach number at peak efficiency point. (For interpretation of the colors in this figure, the reader is referred to the web version of this article.)

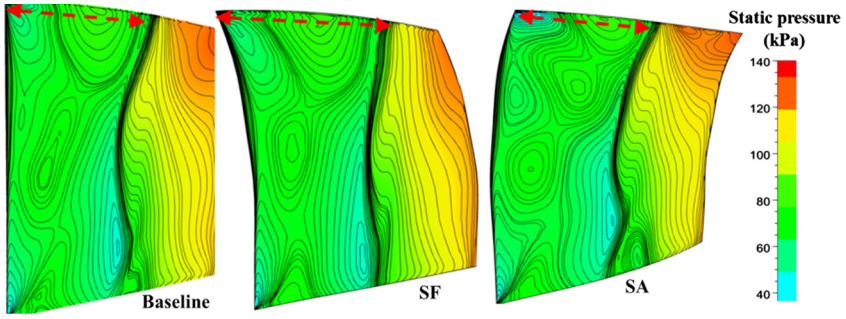

Fig. 13. Static pressure distributions near suction surface at peak efficiency point. (For interpretation of the colors in this figure, the reader is referred to the web version of this article.)

ates in tip gap of rotor SA, and it aggravates the flow blockage in tip region. By contrast, the low-velocity region is much smaller in rotor SF, which is better for flow stability in tip region. In fact, the decrement of shock intensity in tip region of rotor SF not only reduces shock losses and flow separation, but also benefits the stable operation range of compressor in that the weaker passage shock is more farther away from leading edge of rotor at peak efficiency point. In this way, the stall margin of rotor SF has improved obviously.

Fig. 13 illustrates the distribution of static pressure near suction surface at peak efficiency point. It can be seen the shape of passage shock near suction surface presents a little backward sweep over 30% span of three rotors, but the trend of aft-sweep in meridional plane is not as obvious as that in the cascade plane. Besides that, it's also worth noting that the shock front intersects the casing perpendicularly due to the thickened boundary layer near endwall in all three rotors (named as endwall effect). Because of the endwall effects and the spanwise shape of shock front, the location of passage shock in tip region of rotor SF moves downstream and is much closer to the trailing edge, which contributes to a larger stall margin of forward swept rotor (remarked by red dashed segment), while the stall margin of rotor SA has been restricted inevitably.

Fig. 14 presents the limited streamlines near suction surface at peak efficiency point. As the shock front exists in the whole passage in blade span, the local flow separation induced by shock emerges near suction surface of three rotors, and the separation line is consistent with the radial location of shock front. In addition, Fig. 14 shows all the rotors suffer from another new separation near trailing edge in tip region because of negative pressure gradient and sharp change of curvature there. Nevertheless, the

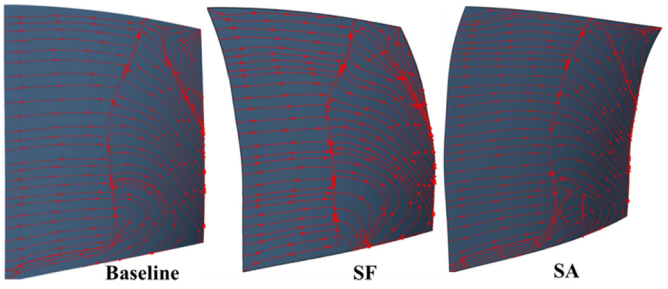

Fig. 14. Limited streamline distribution.

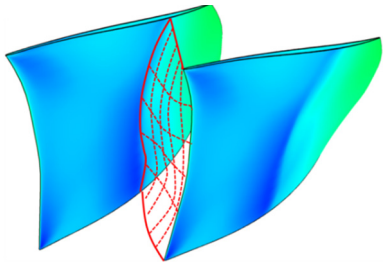

Fig. 15. Three-dimensional structure of shock front at peak efficiency point.

second separation generates near the exit of rotor with almost no obvious influence on main flow, and goes downstream mixing with wake near trailing edge. Considering of the locations of passage shock on both meridional and cascade plane due to aerodynamic sweep, a spatial three-dimensional shock front can be plotted in passage, as shown in Fig. 15.

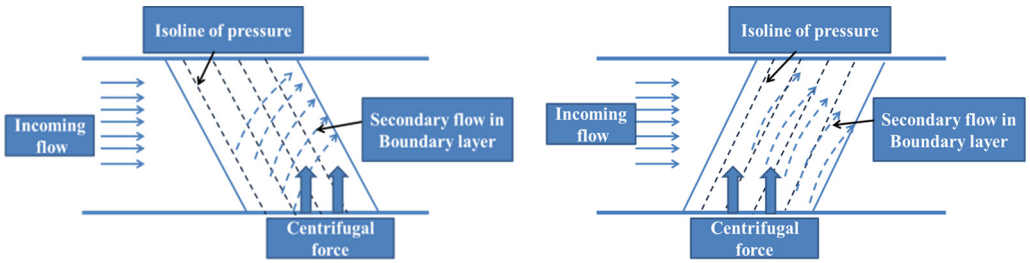

Fig. 16. Sketches of secondary flow near suction surface of blade (Yamaguchi et al. [21]).

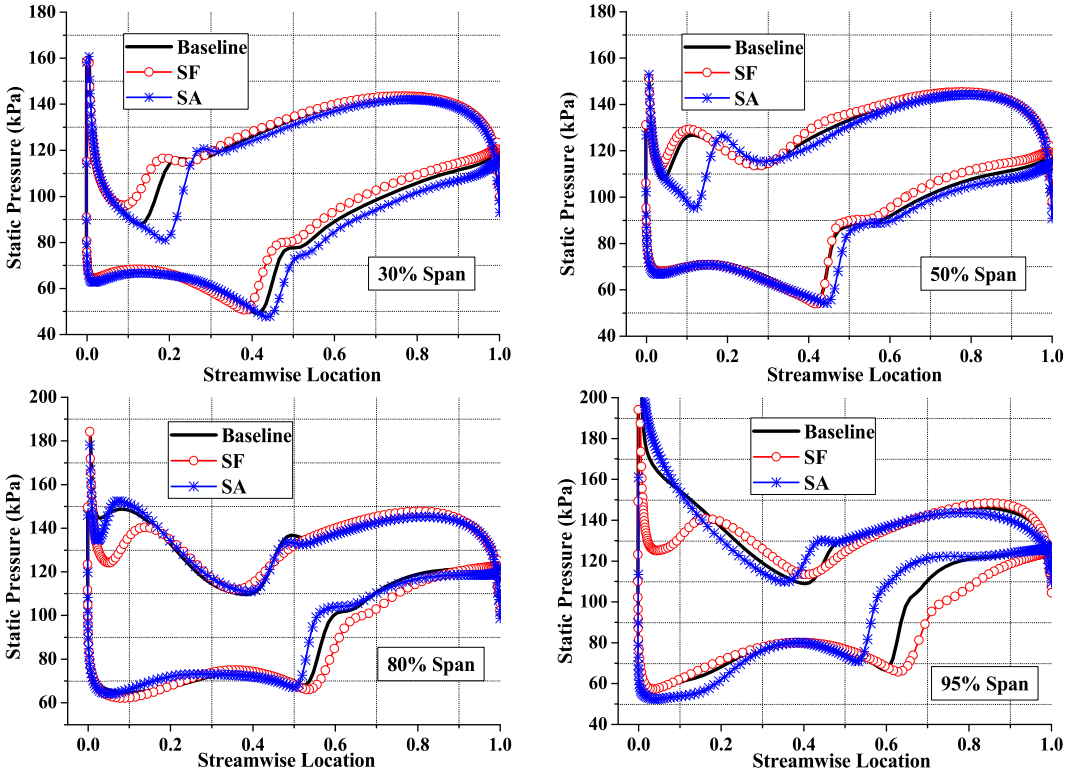

Fig. 17. Streamwise loading distribution at different span of rotors at peak efficiency point.

The limited streamlines in Fig. 14 indicate as well the growing trend of low-energy fluid in boundary layer behind passage shock. Driven by the radial pressure gradient produced by centrifugal force, low-energy fluids in boundary layer transport outward in radial direction from hub to casing, and then accumulate in tip region of blade near suction surface, as shown in Fig. 16. Assuming the loading of rotor at different span remains constant, the leading edge in tip region of forward swept rotor SF meets with incoming flow first and does work to the fluids. Correspondingly, the location of high pressure-region near suction surface goes forward along streamwise in tip region, so a new additional pressure gradient from casing to hub is induced by forward sweep. Because of the new pressure gradient, the existing radial transportation of low-energy fluids driven by centrifugal force of rotating blade has been attenuated in some extent. As a result, the accumulation of low-energy fluids has decreased in tip region of rotor SF, and its location is much closer to the trailing edge as well. All the change of low-energy fluids in tip region of rotor SF is beneficial to suppress the flow blockages in tip region. Different from rotor SF, the accumulation of low-energy fluids increases in tip region of rotor SA due to the opposite pressure gradient induced by aft sweep and its location moves upstream obviously, which aggravates the flow blockage and aerodynamic losses in tip region.

The static pressure distributions near blade surface of three rotors at peak efficiency point are shown in Fig. 17. The loadings near leading edge of rotor SF have improved at 30% and 50% span of blade (especially near pressure side) in comparison with rotor Baseline, while the loadings of rotor SA decrease there. Meanwhile, a little stronger shock moves upstream at 30% and 50% span of rotor SF which corresponds to larger abrupt increase of static pressure, so the losses of shock and separation are a little larger than the other two rotors. However, as the radius of rotor increases from mid-span to casing, the loading distributions of blade along streamwise change obviously due to sweep, which mainly concentrates on the change of shock wave. The strength and location of passage shock affect the stall margin of rotor obviously, and larger distance between shock and leading edge produces wider operation range of compressors. At 80% and 95% span of blade, the shock wave tends to be stronger and goes upstream in rotor SA, and the corresponding blade loading at that span moves forward accordingly. Therefore, all the changes of shock in rotor SA produce larger shock losses and smaller stall margin. Opposite to rotor SA, the passage shocks of rotor SF at 80% and 95% span are much further away from leading edge and its intensity is smaller as well (especially in tip region), which favors better performance and stall margin of rotor SF.

Additionally, an important phenomenon has been predicted in Fig. 17 that the blade loading near leading edge of rotor SF has decreased obviously in tip region compared to other two rotors. It's well known the leakage flow is driven by static pressure difference between two sides of blade and plays an important role in tip region of high loading transonic rotor. Therefore, the decreased loading near leading edge of rotor SF is beneficial to attenuate the strength of leakage flow and its interaction with passage shock, and then reduce flow blockage and losses in tip region. Moreover, the weakened leakage flow does go downstream much closer to suction side and the intersection point of leakage flow with blade surface moves downstream as well, which may reduce the negative effects of leakage vortex on main flow. Fig. 18 shows the trajectory of leakage flow in tip gap of three rotors. It can be seen that the intersection point of leakage flow with suction surface has moved much downstream in rotor SF comparing with the other two rotors. In fact, the more downstream the intersection point moves, the smaller influence and less losses the leakage flow causes, so it's one of the main reasons for better flow characteristics in tip region of rotor SF.

It seems appropriate to conclude that the change of loading distributions in transonic rotors due to aerodynamic sweep relates to two aspects: the change of inflow conditions, and the radial transportation of low-energy fluids in boundary layer. Firstly, aerodynamic sweep has changed the driving force of transportation for low-energy fluids in boundary layer, and affects its accumulation in passage, which has been well illustrated in Fig. 16. The accumulation produces large aerodynamic losses and flow blockage in passage, and affects the location and intensity of shock in turn. Secondly, after utilizing sweep in rotor, the shape of leading edge has changed obviously and a new radial equilibrium reproduces near entrance of blade, so the inlet flow conditions of swept rotors change accordingly. Fig. 19 shows the inlet static pressure and relative Mach number distributions of three rotors at peak efficiency point, there are larger differences existing over 30% span of blades. The static pressure of rotor SF is smaller than rotor Baseline in that region, which is opposite to the distribution in rotor SA. Meanwhile, the spanwise distributions of inlet relative Mach number also have changed a little in three rotors, but the difference is not as larger as the change of static pressure. All the changes of inflow condition contribute to a new flow characteristic of blade airfoil at different span of rotor, and then determine the overall performance of the new swept rotors.

The contours of relative Mach number near stall point in Fig. 20 indicate that, the flowfields in three rotors are similar at this condition. The passage shock has detached upstream away from leading edge, and becomes stronger to be perpendicular to suction surface of blade. The separation flow induced by detached shock strengthens obviously in subsequent passage. In addition, the interactions of leakage flow and passage shock become stronger as well and large low-velocity region appears in tip region. It's one of the key inceptions to stall in highly loaded transonic rotors.

Fig. 21 presents the static pressure distributions on suction surface of three rotors near stall point. Similar to the distributions on cascade plane, the shape of detached shock on meridional surface of three rotors tends to be much perpendicular to endwall, and the strength of shock also increases notably. In addition, the trajectory of leakage flow in tip clearance shown in Fig. 22 indicates that the intersection point of leakage flow with suction surface seems to be close to the leading edge in all three rotors, which also represents a typical characteristic of stall inception in tip region of high loading compressors.

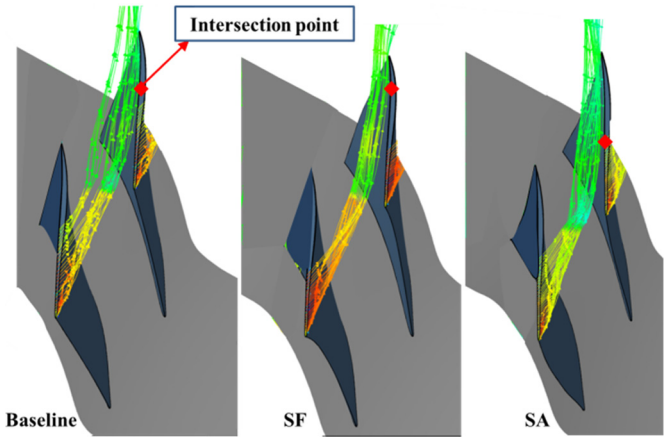

Fig. 18. Trajectory of leakage flow originated from leading edge in rotors at peak efficiency point.

5. Conclusion

Highly loaded transonic rotors with sweep are designed by translating the stacking axis of NASA Rotor 37 in chordwise direction, and the swept rotors are studied by numerical simulation in this paper. The results show both the peak efficiency and total pressure ratio have increased for forward swept rotor SF in comparison with unswept rotor Baseline at peak efficiency point, and its stall margin has improved over 10% as well. By contrast, the overall performance of has decreased for aft swept rotor SA. Meanwhile, the choking massflow of swept rotors changes clearly as a result of the spatial change of aerodynamic throat, and the forward sweep produces a larger area of aerodynamic throat and choking mass flow for blade.

The aerodynamic sweep has different influence on different span of rotor. Therefore, both forward sweep and aft sweep benefit

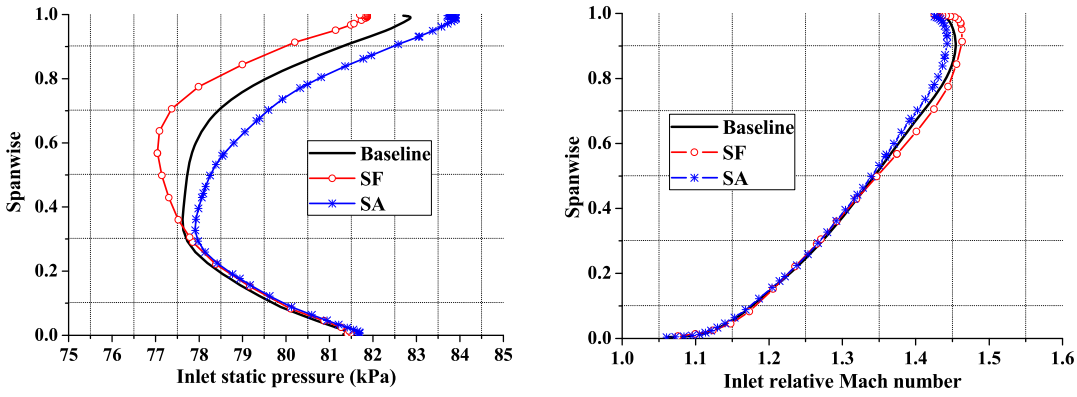

Fig. 19. Inlet conditions of three rotors at peak efficiency point.

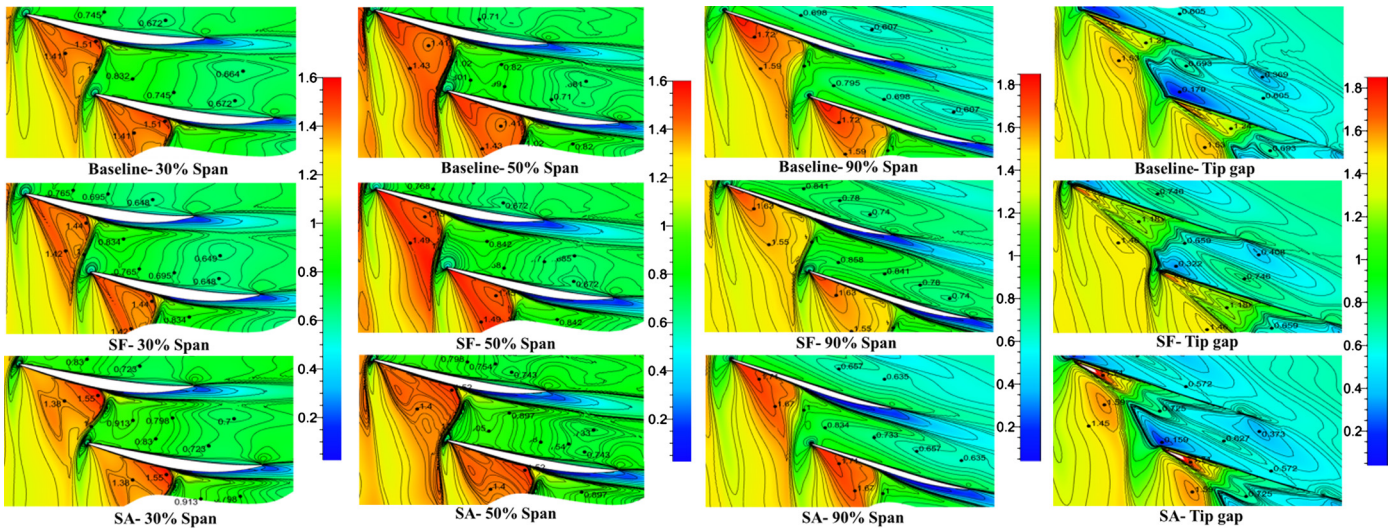

Fig. 20. Distributions of relative Mach number near stall point. (For interpretation of the colors in this figure, the reader is referred to the web version of this article.)

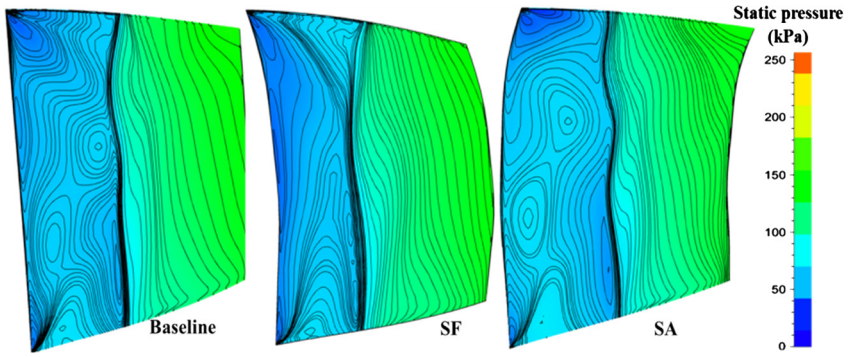

Fig. 21. Static pressure distributions on suction surface. (For interpretation of the colors in this figure, the reader is referred to the web version of this article.)

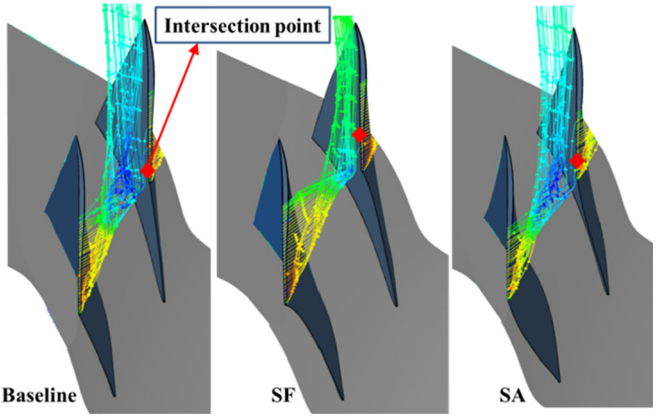

Fig. 22. Trajectory of leakage flow originated from leading edge in rotors near stall point near stall point.

to flow characteristic improvement in a certain span of swept rotors, which affects new radial and streamwise loading distributions in swept rotors. The additional radial pressure gradient produced by forward sweep attenuates the accumulation of low-energy fluids, which weakens the passage shock in tip region and pushes the shock front far away from leading edge of blade. Meanwhile, the strength of leakage flow is also suppressed because of the decreased loading near leading edge in tip region of the forward swept rotor. Therefore, the aerodynamic losses and flow blockage in tip region has decreased obviously in the forward swept rotor SF and its stall margin is also improved.

The aerodynamic sweep has changed the inflow conditions and the characteristic match of each blade airfoil at different span of rotors. First, because of the new radial equilibrium near leading edge induced by sweep, the inlet static pressure and relative Mach number present new distributions in spanwise direction. Second, as the inlet conditions change in swept rotors, the flow characteristic of each blade airfoil in span changes accordingly, especially the 3-D shock structure. Therefore, the characteristic of blade airfoil at different span present a new radial match for rotor, which determines the overall performance of the whole swept rotors directly.

Conflict of interest statement

The authors declare that there is no conflict of interest.

Acknowledgements

This work has been carried out with the support of National Natural Science Foundation of China (No. 51306175). The authors sincerely thank it for funding this work.

References

[1] D.K. Broichhausen, U.K. Ziegler, Supersonic and transonic compressors: past, status and technology trends, ASME paper GT2005-69067, 2005.
[2] N. Takahiro, J. Masayoshi, Characteristics of tip leakage flow at high stagger-angle setting for rotor blade in an axial flow fan, ASME paper GT2012-69204, 2012.
[3] F. Lin, J. Du, J.Y. Chen, C.Q. Nie, B. Christoph, Flow structure in the tip region for a transonic compressor rotor, ASME paper GT2010-23025, 2010.

[4] C. Hah, D.C. Rabe, Role of tip – leakage vortices and passage shock in stall inception in a swept transonic compressor rotor, ASME paper GT2004-53867, 2004.
[5] K. Yamada, K. Funazaki, H. Sasaki, Numerical investigation of relation between unsteady behavior of tip leakage vortex and rotating disturbance in a transonic axial compressor rotor, ASME Paper GT2008-50779, 2008.
[6] C. Hah, A.J. Wennerstrom, Three dimensional flowfields inside a transonic compressor with swept blades, ASME J. Turbomach. 113 (2) (1991) 241–251.
[7] M. Braun, J.R. Seume, Forward sweep in a four-stage high-speed axial compressor, ASME paper GT2006-90218, 2006.
[8] J. Gunaraj, David Hanson, J. Hayes, H. Lorzel, et al., A comparison of two fan stage designs with different rotor leading edge sweep, ASME paper 2014-27218, 2014.
[9] S.G. Mcnulty, J.J. Decker, B.F. Beacher, S.A. Khalid, The impact of forward swept rotors on tip-limited low-speed axial compressors, ASME J. Turbomach. 126 (4) (2004) 445–454.
[10] L.C. Ji, J. Chen, Review and understanding on sweep in axial compressor design, ASME paper GT2005-68473, 2005.
[11] L.A. Beatty, M. Savage, J.C. Emerry, Low, Speed cascade tests of two 45 degree swept compressor blades with constant spanwise loading, NACA RM-L53L07, 1954.
[12] W.R. Goldwin, Effect of sweep on performance of compressor blade sections as indicted by swept blade rotor, unswept blade rotor and cascade tests, NACA TN-4062, 1957.
[13] L.H. Smith, H. Yeh, Sweep and dihedral effect in axial flow turbomachinery, ASME J. Basic Eng. 85 (3) (1963) 401–416.
[14] D.B. Bliss, R.E. Hayden, B.S. Murray, P.G. Schwer, Design considerations for a novel low source noise transonic fan stage, AIAA paper 76-577, 1976.
[15] J.P. Gostelow, L.H. Smith, Aerodynamic design and performance of a swept back rotor SW-1, GE Internal report 68-AEG-175, 1968.
[16] C. Hah, S.L. Puterbaugh, A.R. Wadia, Control of shock structure and second flow inside transonic compressor rotors through aerodynamic in sweep, ASME paper 98-GT-561, 1998.
[17] J. Bergner, S. Kablitz, D.K. Hennecke, Influence of sweep on the 3d shock structure in an axial transonic compressor, ASME paper GT2005-68835, 2005.
[18] P. Shan, X.Y. Liu, Y.H. Luo, Analysis of the aerodynamic behavior of the swept leading edge shock surfaces in high loading axial flow compressors, ASME paper GT-0353, 2001.
[19] A.R. Wadia, P.N. Szucs, D.W. Crall, Inner workings of aerodynamic sweep, ASME J. Turbomach. 120 (4) (1998) 671–682.
[20] J.D. Denton, L. Xu, The effects of lean and sweep on transonic fan performance, ASME paper GT-2002-30327, 2002.
[21] N. Yamaguchi, T. Tominaga, S. Hattori, T. Mitsubishi, Secondary-loss reduction by forward-skewing of axial compressor rotor blading, in: Proceedings of 1991 Yokohama International Gas Turbine Congress, vol. 2, 1991, pp. 61–68.
[22] P.V. Ramakrishna, M. Govardhan, Combined effects of forward sweep and tip clearance on the performance of axial flow compressor stage, ASME paper GT2009-59840, 2009.
[23] T. Sasaki, F. Breugelmans, Comparison of sweep and dihedral effects on compressor cascade performance, ASME paper 97-GT-2, 1997.
[24] H. Watanabe, M. Zangeneh, Design of the blade geometry of swept transonic fans by 3D inverse design, ASME paper GT2003-38770, 2003.
[25] O. Hidetaka, V. Tom, Three dimensional design and optimization of a transonic rotor in axial flow compressors, ASME paper GT2011-45425, 2011.
[26] M.A. Aziz, F.M. Owis, Abdelrahman, Design optimization of a transonic-fan rotor using numerical computations of the full compressible Navier–Stokes equations and simplex algorithm, Int. J. Rotating Mach. 2014 (2014) 743154, http://dx.doi.org/10.1155/2014/743154.
[27] N.I. Ayhan, A. Erkan, Influence of the sweep stacking on the performance of an axial fan, ASME J. Turbomach. 137 (6) (2015) 061004, http://dx.doi.org/10.1115/1.4028767.
[28] V. Janos, Forward blade sweep applied to low-speed axial fan rotors of controlled vortex design: an overview, ASME J. Eng. Gas Turbines Power 135 (1) (2013) 012601.
[29] R.R. Seyed, B. Masoud, Numerical and performance analysis of one row transonic rotor with sweep and lean angle, J. Therm. Sci. 23 (5) (2014) 438–445.
[30] C. Hah, H.W. Shin, Study of near-stall flow behavior in a modern transonic fan with compound sweep, J. Fluids Eng. 134 (7) (2012) 071101.
[31] E. Benini, R. Biollo, On the aerodynamics of swept and leaned transonic compressor rotors, ASME paper GT2006-90547, 2006.
[32] NUMECA International, Theoretical manual, 2009.
[33] J. Dunham, CFD validation for propulsion system components, AGARD-AR-355, 1998.
[34] L. Reid, R.D. Moore, Design and overall performance of four highly loaded high-speed inlet stages for an advanced high-pressure-ratio core compressor, NASA-TP-1337, 1978.